Experimental data from a full-scale facility investigating radiant and convective terminals

Uncertainty and sensitivity analysis, Description of the experimental data

Le Dreau, Jerome; Heiselberg, Per; Jensen, Rasmus Lund

Publication date:
2014

Document Version
Publisher's PDF, also known as Version of record

Experimental data from a full-scale facility investigating radiant and convective terminals

Uncertainty and sensitivity analysis, Description of the experimental data

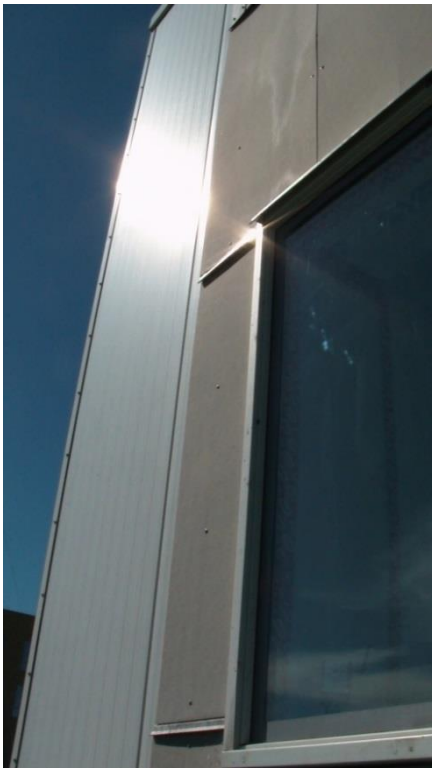

Jérôme Le Dréau
Per Heiselberg
Rasmus Lund Jensen

ISSN 1901-726X
DCE Technical Report No. 168

DEPARTMENT OF CIVIL ENGINEERING
AALBORG UNIVERSITY

Aalborg University
Department of Civil Engineering
Architectural Engineering

DCE Technical Report No. 168

Experimental data from a full-scale facility investigating radiant and convective terminals

Uncertainty and sensitivity analysis, Description of the experimental data

by

Jérôme Le Dréau
Per Heiselberg
Rasmus Lund Jensen

April 2014

Scientific Publications at the Department of Civil Engineering

Technical Reports are published for timely dissemination of research results and scientific work carried out at the Department of Civil Engineering (DCE) at Aalborg University. This medium allows publication of more detailed explanations and results than typically allowed in scientific journals.

Technical Memoranda are produced to enable the preliminary dissemination of scientific work by the personnel of the DCE where such release is deemed to be appropriate. Documents of this kind may be incomplete or temporary versions of papers—or part of continuing work. This should be kept in mind when references are given to publications of this kind.

Contract Reports are produced to report scientific work carried out under contract. Publications of this kind contain confidential matter and are reserved for the sponsors and the DCE. Therefore, Contract Reports are generally not available for public circulation.

Lecture Notes contain material produced by the lecturers at the DCE for educational purposes. This may be scientific notes, lecture books, example problems or manuals for laboratory work, or computer programs developed at the DCE.

Theses are monograms or collections of papers published to report the scientific work carried out at the DCE to obtain a degree as either PhD or Doctor of Technology. The thesis is publicly available after the defence of the degree.

Latest News is published to enable rapid communication of information about scientific work carried out at the DCE. This includes the status of research projects, developments in the laboratories, information about collaborative work and recent research results.

Published 2014 by
Aalborg University
Department of Civil Engineering
Sohngaardsholmsvej 57
DK-9000 Aalborg, Denmark

Printed in Aalborg at Aalborg University

ISSN 1901-726X
DCE Technical Report No. 168

Recent publications in the DCE Technical Report Series

Table of content

Introduction

The objective of this technical report is to provide information on the accuracy of the experiments performed in "the Cube" (part I, II and III). More general information about the experimental set-up and results can be found in [1] and in [2].
Moreover, this report lists the experimental data, which have been monitored in the test facility (part IV). These data are available online and can be used by other researchers.

In this report, different uncertainty analyses are conducted. It should be noted that the values given are specific to this set-up and cannot be used as such if the experimental conditions are different. Nevertheless, the methodology can be applied to similar set-up.
All uncertainties specified in this report are given for a confidence interval of 95% (2σ), normally distributed. The uncertainty has two components, namely, bias (related to accuracy) and the unavoidable random variation that occurs when making repeated measurements (related to precision) [3].

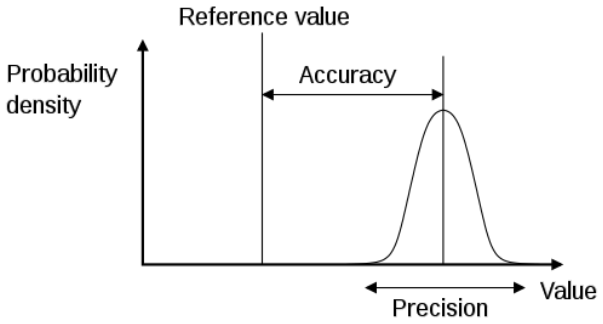

Figure 1: Difference between accury and precision [3].

I. Uncertainty of measurements

1) Type K thermocouples

The uncertainty of measurements with type K thermocouples will first be evaluated theoretically using the rules of propagation of uncertainty and will then be observed experimentally. The uncertainty depends on the calibration (highlighted by a blue colour), but also on the accuracy of the different measuring equipment.

Introduction

The accuracy limits of different temperature sensors are given in Table 1. It has to be noted that these accuracies are used only when an individual calibration is not performed.

Table 1: Nominal accuracy of temperature sensors.

Type	Sensitivity	Nominal class 1 or A	Nominal class 2 or B	Reference
Thermocouples Type K	41 µV/°C	± 1.5°C	± 2.5°C	EN-60584-3
Thermocouples Type T	43 µV/°C	± 0.5°C	± 1.0°C	EN-60584-3
Pt-100	0.385 Ω/°C	± 0.15°C	± 0.3°C	EN-60751

The uncertainty of temperature measurement in different experimental set-ups has been summarised in the table below (Table 2). It can be observed that the uncertainty varies much with the set-up, but few details are provided to explain these different values (type of temperature sensor, logging system, etc). A detailed analysis will thus be performed to investigate the uncertainty of the specific experimental set-up.

Table 2: Uncertainty of temperature measurements in the literature [4].

Type		Accuracy	Reference
Thermocouples	Type T	± 0.1°C	KU Leuven - Belgium
	Type T	± 0.1°C	NRC - Canada
	Type T (combined with HP Agilent 34982A)	± 0.4°C	Engineering School of Bilbao - Spain
	Type T	± 0.1°C	CSTB - France
	Type T	± 0.3°C	EMPA - Switwerland
	Type T	± 0.19°C	Ghent University - Belgium
	Type T (combined with Keithley 7200)	± 0.6°C	INSA Lyon - France
	Type K (combined with Keithley 7200)	± 0.3°C	INSA Lyon - France
	Type K (combined with Fluke Helios 2287)	± 0.09°C	Aalborg University - Denmark
Pt 100	Pt 100	± 0.1°C	Fraunhofer Institute - Germany
	Pt 100 (DIN EN 60751 Class B)	± 0.3°C	Fraunhofer Institute IBP - Germany
	Pt 100 (class A, 1/5 DIN, combined with HP Agilent 34982A)	± 0.2°C	Engineering School of Bilbao - Spain
	Pt 100 (1/3 DIN 4-wires)	± 0.05°C	CSTB - France
	Pt 100 (combined with Keithley 7200)	± 0.2°C	INSA Lyon - France
	Pt 100 (combined with Beckhoff EL3202-0010)	± 0.15°C	Tecnalia - Spain

Measurement set-up

In this experimental set-up, surface temperature measurements are performed using type K thermocouples. All thermocouples are connected to a compensation box; the temperature of the compensation box is recorded by 4 reference thermocouples, which are connected to an ice-point reference (Figure 2). Each thermocouple has been calibrated individually.

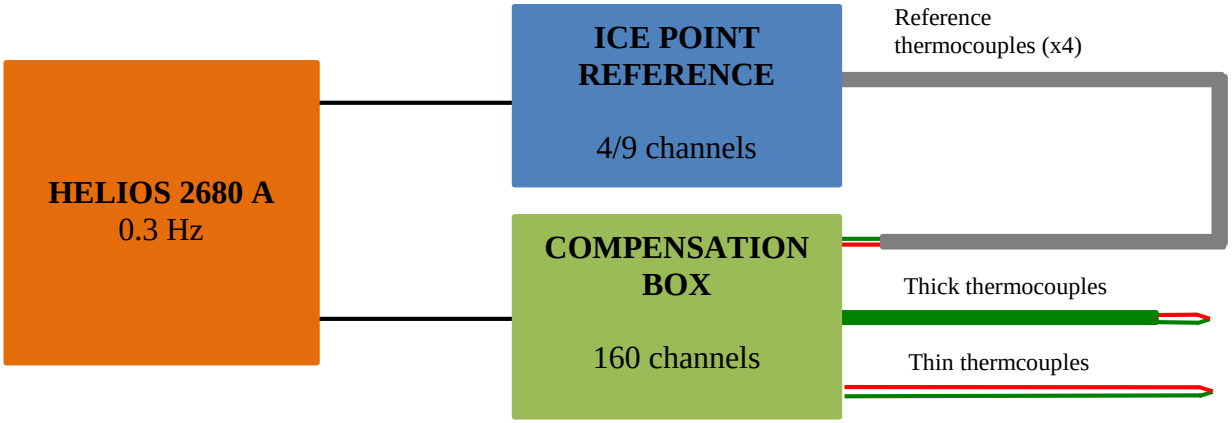

Figure 2: Data logger and measuring equipment.

Calculated uncertainty

The uncertainty of surface temperature measurement is the sum of 4 terms: the measurement error of the temperature of the compensation box ($\Delta T_{IPR\text{-}CB}$), the homogeneity of the compensation box (ΔT_{CB}), the measurement error of the thermocouple ($\Delta T_{CB\text{-}P}$) and finally the installation error ($\Delta T_{installation}$). In this first part, the installation error will not be considered.

$$\Delta T = \sqrt{\Delta T_{IPR-CB}{}^2 + \Delta T_{CB}{}^2 + \Delta T_{CB-P}{}^2 + \Delta T_{installation}{}^2}$$

$$= \begin{cases} \sqrt{0.15^2 + \Delta T_{installation}{}^2}\ K & \text{for a second order calibration} \\ \sqrt{0.20^2 + \Delta T_{installation}{}^2}\ K & \text{for a first order calibration} \end{cases} \qquad (1)$$

This uncertainty calculation is valid under precise conditions:

- similar set-up and measurement equipment
- yearly calibration of the equipment
- individual calibration of the thermocouples
- four thermocouples measuring the compensation box temperature (located in different blocks of the data logger or different data loggers)

- Uncertainty on the temperature difference between the ice point reference and the compensation box (measured by $n_{ref\ TC} = 4$ thermocouples)

$$\Delta T_{IPR-CB} = \sqrt{0.026^2 + 0.006^2 + \frac{0.004^2 + 0.020^2 + 0.12^2 + 0.020^2}{n_{ref\ TC} - 1}} = 0.077\ K \qquad (2)$$

  - CALIBRATION - Reference thermometer used for calibration (F200 Tinsley – ASL) [5]: ± 0.006 K (maximum correction step between 10 and 50°C)
  - CALIBRATION - Homogeneity of the isocal box (Venus 2140 B) with metal block [6]: ± 0.004 K
  - CALIBRATION - Automatic Ice Bath (Kaye K170) [7]: ± 0.020 K
  - CALIBRATION - Fitting of the calibration curve (calibration 10 to 50°C): ± 0.026 K with a 2nd order polynomial or ± 0.083 K with a 1st order polynomial (Figure 3). The voltage output of type K thermocouples is based on the thermocouple database of the U.S. National Institute of Standards and Technology (NIST) [8].

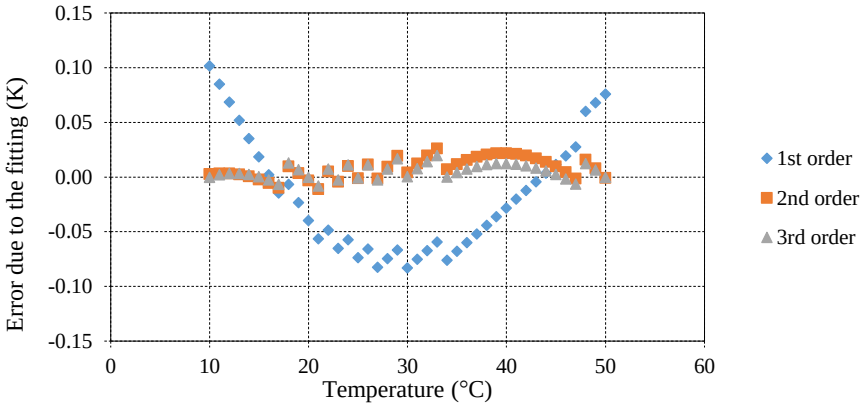

Figure 3: Error on the curve fitting depending on the order of calibration (6 calibration points at 10°C, 15°C, 20°C, 25°C, 30°C and 50°C).

  - Automatic Ice Bath (Kaye K170) [7]: ± 0.020 K

  - Accuracy of the data logger Fluke Helios 2680 PAI slow ($3\sigma = 0.01\% + 7\ \mu V$, with an input voltage of 1.40 mV at 35°C) [9].
    This value is valid is valid if the data logger is kept at a temperature between 18 and 28°C and includes the AD errors, the linearization conformity, the initial calibration error, the drift in time and in space. When performing individual calibration, some of these errors are reduced (e.g. initial calibration error or offset in space), but it is difficult to get an accurate estimation of the remaining error. Therefore, the value given by the manufacturer has been kept without modification.

$$\frac{2}{3} \cdot \left(\frac{0.01}{100} \cdot V_{input} + 7 \right) = 4.76\ \mu V \approx 0.12\ K$$

    Additionally, this value has been compared to the drift observed on the data logger from the laboratory. Every year, the accuracy of the voltage measurement is checked. The yearly changes can thus be monitored (Figure 4). It can be observed that the accuracy of the data logger is within the range given by the manufacturer, except for the data logger number 233, where a sudden change has been observed between 1997 and 1998.

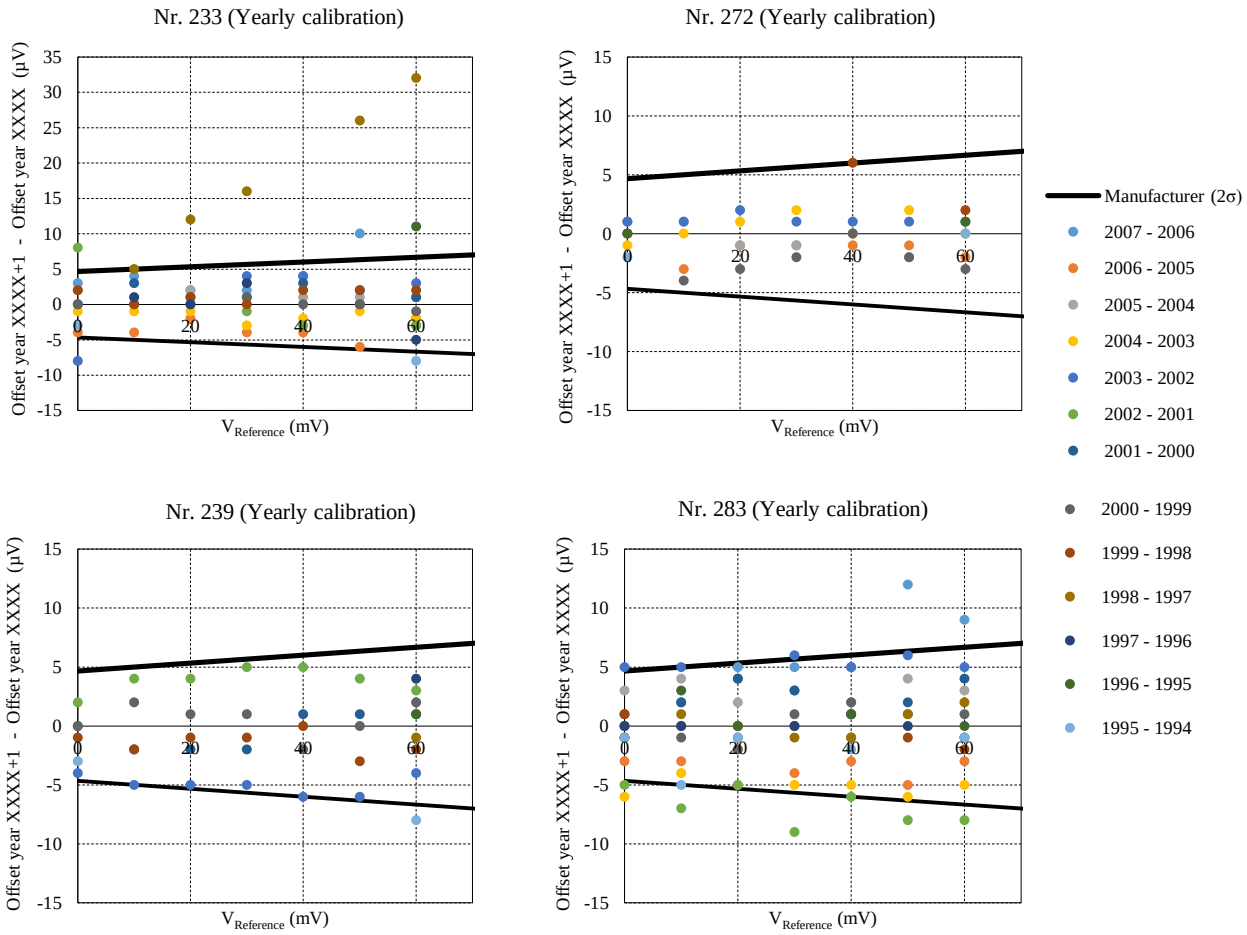

Figure 4: Yearly changes in the voltage offset of Fluke Helios 2287 PAI data loggers (range ± 64 mV).

It can be observed that the offset is changing over the time and does not follow any trend. Artmann et al. [10] also observed that the offset was not constant, even for a short period of time. It was varying "between 1.7 and 7.9 µV […]. However, the accuracy of the measurements was not found to be improved when the offsets were subtracted from the measured signals".

In order to decrease the effect of this offset on the temperature measurement of the compensation box, the 4 reference thermocouples have been placed in different blocks. Another way of decreasing the offset is to place the reference thermocouples in two different data loggers. In this experimental set-up, the reference thermocouples were place in different blocks, but in the same data-logger.

- Temperature difference between the different channels of the compensation box:
  The performance of the compensation box has been estimated by applying a temperature step of 2 K in a climatic chamber. The maximum temperature difference measured between different channels is: $\Delta T_{CB} = \pm 0.005$ K [10].

- Uncertainty in the temperature difference between the compensation box and the measurement point P:

$$\Delta T_{CB-P} = \sqrt{0.006^2 + 0.004^2 + 0.028^2 + 0.12^2} = 0.122\ K \qquad (3)$$

  - CALIBRATION - Reference thermometer used for calibration (F200 Tinsley – ASL) [5]: ± 0.006 K
  - CALIBRATION - Homogeneity of the isocal box (Venus 2140 B) with metal block [6]: ± 0.004 K
  - CALIBRATION - Fitting of the calibration curve (calibration -10 to 30°C): ± 0.028 K with a 2nd order polynomial, or ± 0.119 K with a 1st order polynomial (Figure 5)

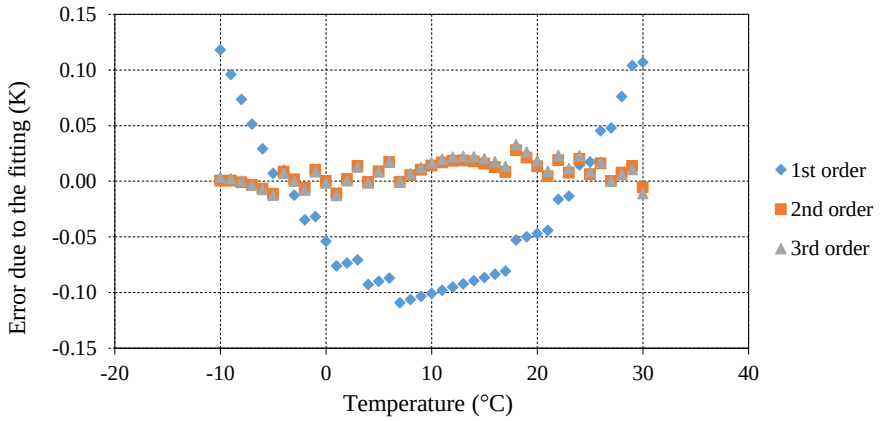

Figure 5: Error on the curve fitting depending on the order of calibration (4 calibration points at -8°C, -3°C, 7°C and 27°C).

It has to be noticed that a first order calibration can be accurate enough, when only positive values are expected (Figure 6): the resulting accuracy on the fitting is then ± 0.035 K.

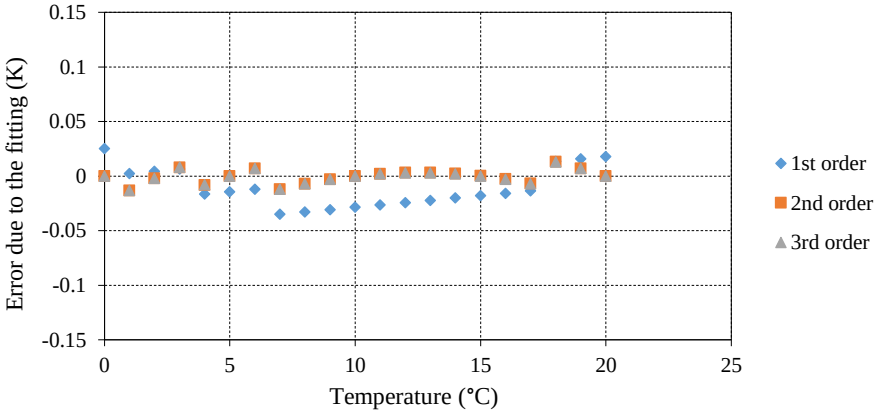

Figure 6: Error of the fitting is ONLY positive values are expected (4 calibration points at 0°C, 5°C, 10°C and 20°C).

- Accuracy of the data logger Fluke Helios 2680 PAI slow (input voltage of 1.199 mV at 30°C) [9]

$$\frac{2}{3} \cdot \left(\frac{0.01}{100} \cdot V_{input} + 7 \right) = 4.75\ \mu V \approx 0.12\ K$$

Experimental validation of the uncertainty

In order to observe the difference between a first and second order calibration, an experiment has been conducted with 14 thermocouples, after calibrating each of them individually. The 14 thermocouples are divided in three different types: 6 thin, 6 thick silver coated and 2 thick non-silver coated thermocouples. They are connected at different locations of the compensation box and are associated either to the data logger Helios 2680A or Helios 2287A.

The 14 thermocouples are placed in a metallic box (Figure 7) for 50 hours, but only the values after 24 hours are presented in this document. Similar results were obtained at other time of the experiment. The temperature of the metallic box is equal to 17±1°C. Thermal paste has been applied to all thermocouples in order to ensure a good contact with the metallic box. The logging frequency is every 5 seconds for Helios 2680A and every 10 seconds for Helios 2287A. A moving average over 9 values is performed to analyse the data (in order to remove the noise).

Figure 7: Thermocouples and metallic box used during the test (upper part of the shield removed).

The true temperature of the metallic box is assumed to be equal to the average value of the 14 thermocouples obtained with a second-order calibration. The experimental results are then compared to the uncertainty band, calculated according to Equation 1 and taking into account the inhomogeneity of the metallic box (ΔT_{CB} = *0.005* K).

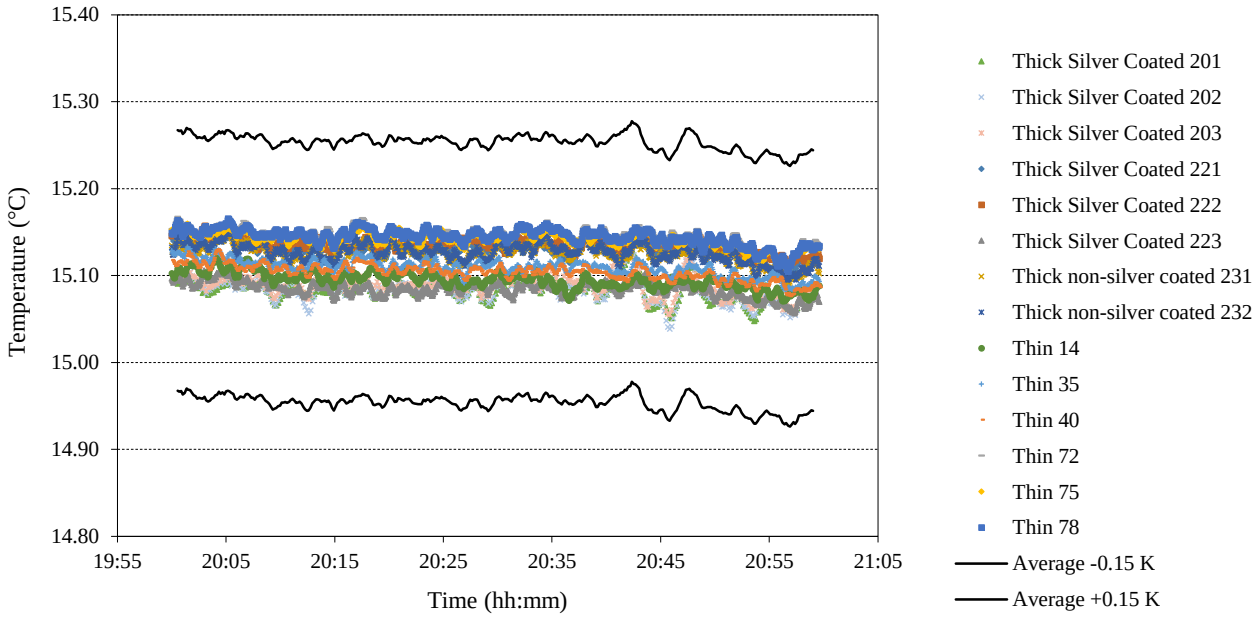

Figure 8: Temperature obtained experimentally after a second-order calibration and compared with the calculated uncertainty (black lines).

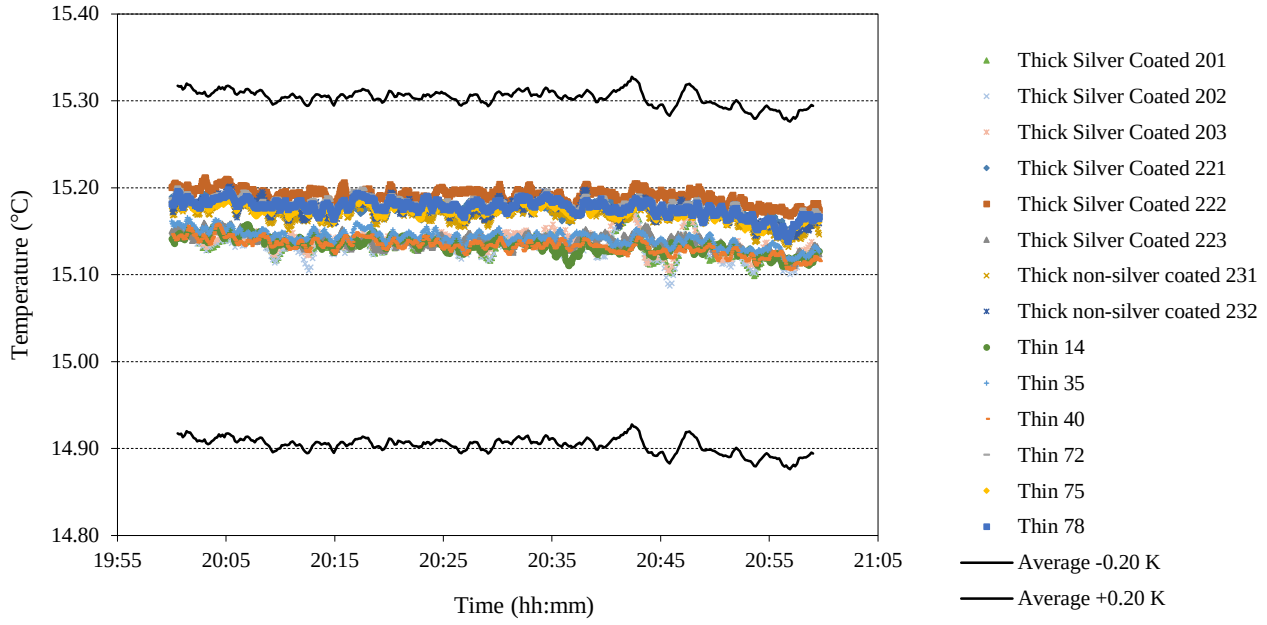

Figure 9: Temperature obtained experimentally after a first-order calibration and compared with the calculated uncertainty (black lines)

The results are given for a second-order calibration in Figure 8, and for a first-order calibration in Figure 9. It can be observed that the bias component dominates over the precision due to the large uncertainty of the data logger (0.12 K). Additionally, the second order calibration proved to decrease the uncertainty of measurement (by approximately 0.05 K in this case).

Conclusion

The uncertainty of a temperature measurement performed with such an experimental set-up is thus equal to ± 0.15 K. The importance of performing a second-order calibration has been proved (Figure 8). Nevertheless, the offset is playing an important role in the uncertainty of type K thermocouples due to the low amplitude of the output signal.

In a previous report [10], Artmann et al. estimated the uncertainty of thermocouple measurements equal to ± 0.086 K. The discrepancy can be explained by differences in the evaluation of propagation of uncertainty, in the calibration technique, and also in the evaluation of the offset.

2) Installation error of surface temperature sensors

The installation error ($\Delta T_{installation}$) should account for different parameters. Some of the parameters can be neglected, such as:

- The contact resistance between surface and thermocouple. Thermal paste has been used to maximise the conductive heat flux around the thermocouple (Figure 10)
- The modification of the radiative heat flux. After being mounted on the wall, the sensor has been painted. The optical properties of the surface of interest are thus similar to the thermocouple.
- The modification of the convective flow due to the thermocouple. By using thin thermocouples mounted horizontally, the convective flow is not much disturbed around the area of measurement.

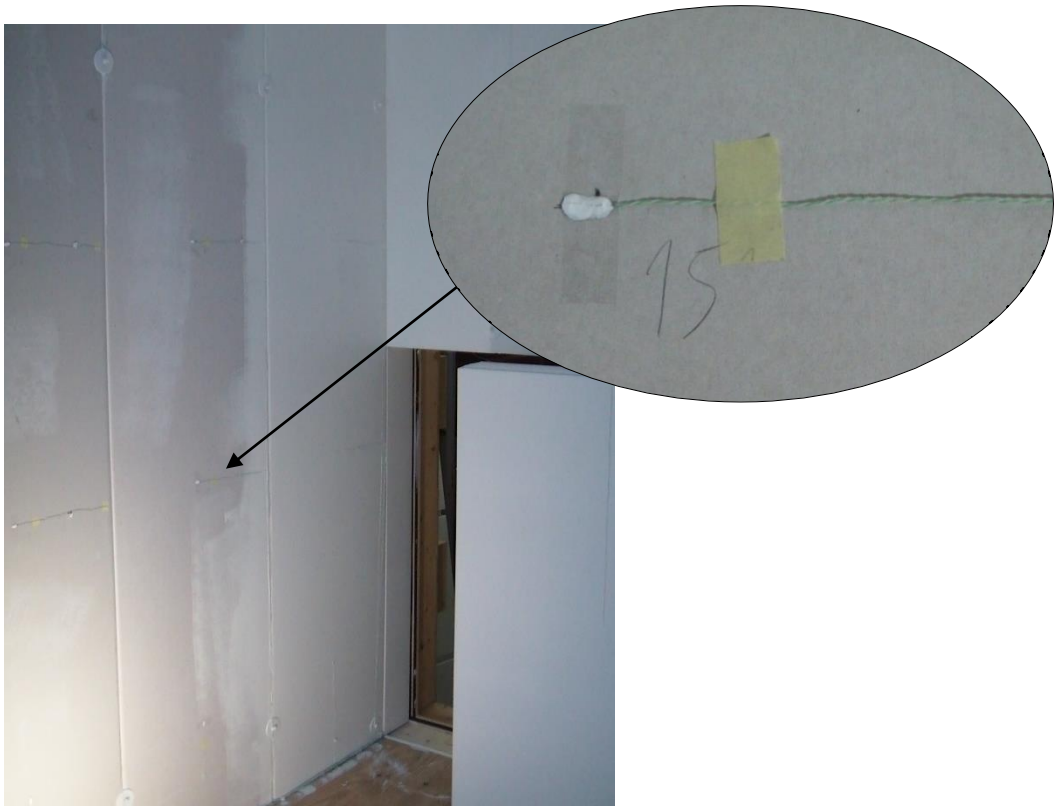

Figure 10: Thermocouples mounted on the wall (before being painted).

Some other parameters cannot be neglected and need to be assessed.
The homogeneity of the surface temperature has been taken into consideration by testing different interpolation techniques. In fact, the surface temperature is measured only at a limited number of positions and is then assumed to be representative of the entire section. Therefore, simulations using the experimental data have been performed to evaluate the influence of the type of extrapolation on the average surface temperature (linear, cubic, natural neighbour [11]). The largest variation has been observed at the ceiling, where the difference is up to 0.20 K.

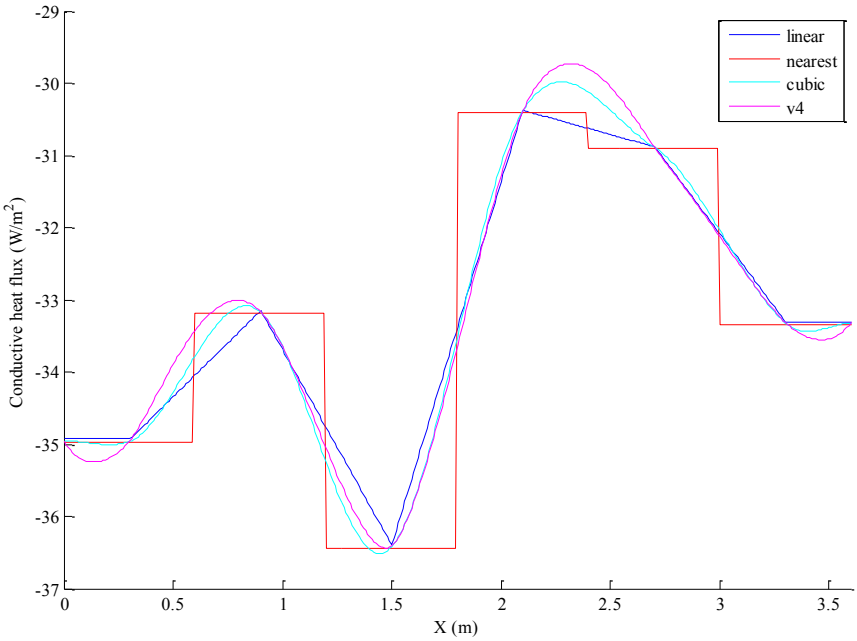

Figure 11: Example of interpolation techniques tested (cross section of the west wall).

3) Air temperature

With solar radiation:

To measure the air temperature distribution in the room, five columns of thermocouples have been installed in the test room: one in the middle and one in the centre of each wall. The thermocouples are recording air temperature at 0.1, 0.6, 1.1, 1.7 and 2.65 m high. In order to decrease the influence of radiation on the measurement of air temperature, the thermocouples are silver-coated and protected by a silver-shield mechanically ventilated (Figure 12).

Figure 12: Air temperature measurement.

This type of sensor has been chosen based on the study from Kalyanova et al. [12, 13]. In their study, they tested different types of sensors and pointed out the effect of solar radiation: "the presence of direct solar radiation […] can heavily affect measurements of air temperature and may lead to errors of high magnitude using bare thermocouples and even adopting shielding devices". The air velocity around the thermocouple also plays an important role: "mechanically ventilated (single) shielding devices provide better results than naturally ventilated ones".
Nevertheless, no detailed calculation of the uncertainty of such device can be found in the literature. Kurzeja [14] mentions that "[temperature sensors within mechanically-aspirated, shaded, multi-walled tubes] are commonly assumed to have negligible error (< 0.1 K)".

The temperature measured by the thermocouple is the average of the radiant and air temperature [15]:

$$T_{TC} = \frac{h_{conv} \cdot T_{air} + h_{rad} \cdot T_{rad}}{h_{conv} + h_{rad}} \qquad (4)$$

An ideal air temperature sensor would be characterised by either $h_{rad} = 0$ or $h_{conv} = \infty$. The measurement error has been estimated by establishing the shield and the thermocouple heat balance under different conditions. The assumptions are the following:

- The thermocouple is adiabatic
- Half of the shield is directly heated by solar radiation
- There is no short-wave radiation directly on the thermocouple
- The long-wave radiative exchange between different parts of the shield has been neglected (i.e. homogeneous temperature of the shield).
- The flow in the shield is laminar fully developed (fan speed of 1.5 m/s).

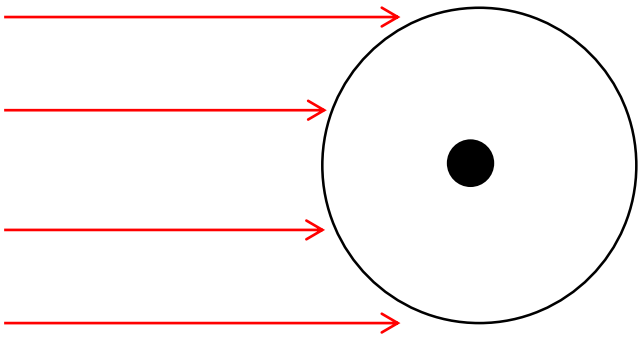

Shield:
$h_{conv\ out}$ = 2.5W/m².K [22]
$h_{conv\ in}$ = 3.8W/m².K [24]
α = 0.20
ε = 0.06

Thermocouple:
h_{conv} = 44W/m².K @ 1.5 m/s
18W/m².K @ 0.2 m/s [23]
ε = 0.06

Figure 13: Top view of the thermocouple, the shield and the incoming solar radiation (in red). The boundary conditions for the calculation are given in the table on the right.

The radiative exchange is calculated assuming concentric spheres. The results from the heat balance are shown in Figure 14 (fan speed of 1.5 m/s) and Figure 15 (fan speed of 0.2 m/s). Similarly to the results obtained experimentally by Kalyanova et al. [12, 13], it has been observed that the fan speed plays an important role on the measurement error.

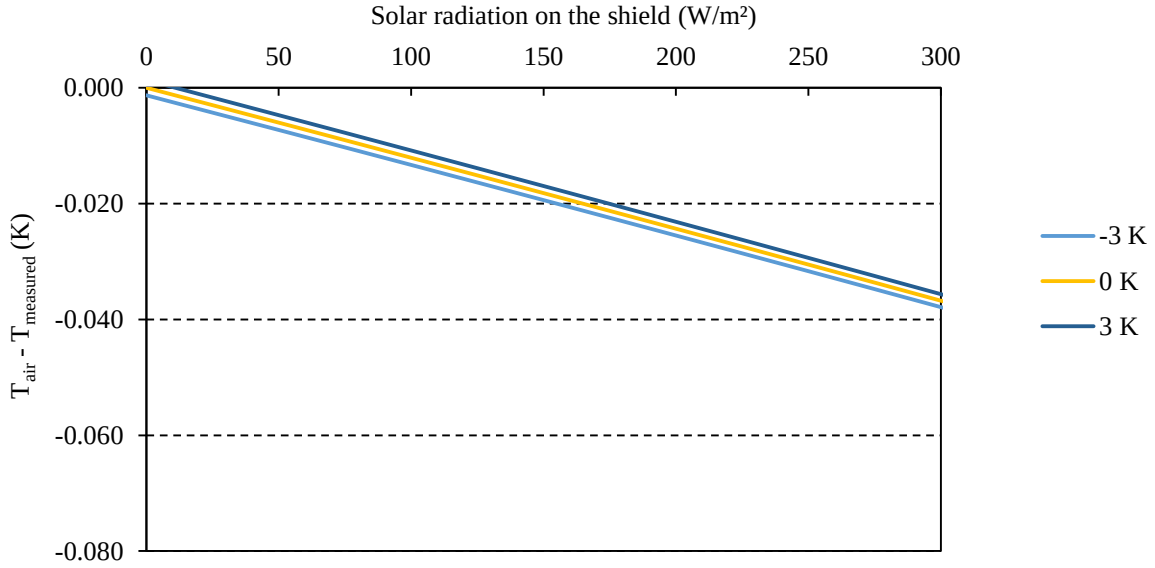

Figure 14: Difference between measured and air temperature for various solar condition (x-axis) and various temperature differences between the air and the room surfaces (legend). Fan speed 1.5 m/s.

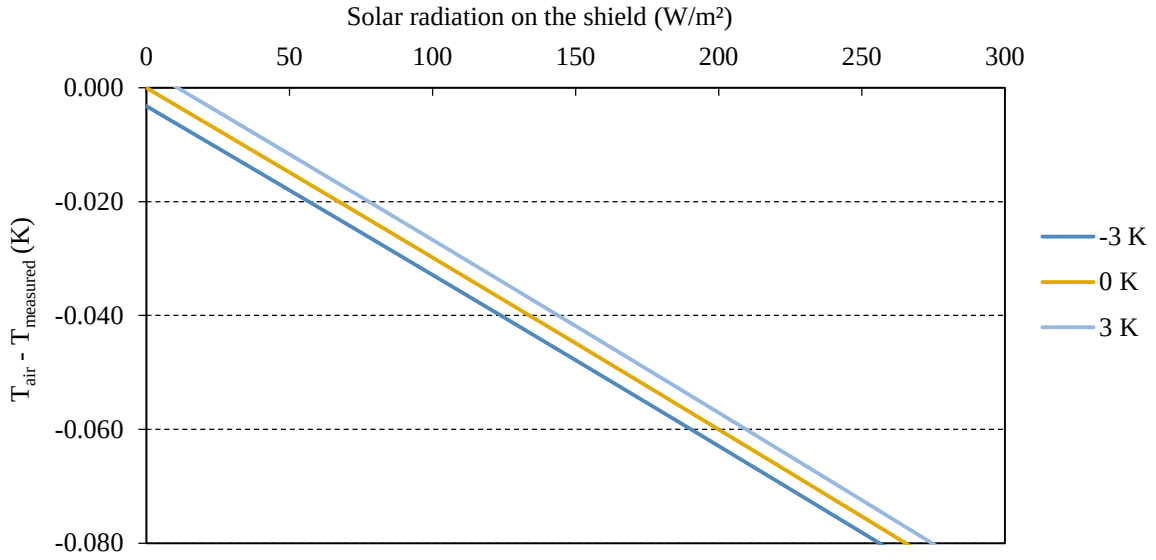

Figure 15: Difference between measured and air temperature for various solar condition (x-axis) and various temperature differences between the air and the room surfaces (legend). Fan speed 0.2 m/s.

The uncertainty of air temperature measurement can be simplified by Equation 5 (for a fan speed of 1.5 m/s). It should be noted that this value does not account for the thermocouple uncertainty, which should be accounted for using the method developed in the previous chapter (I.1).

$$\Delta T_{air} = -1.23 \cdot 10^{-4} \cdot q_{SW\ vert\ inside} + 3.51 \cdot 10^{-4} \cdot \left(T_{air} - T_{surfaces}\right) \quad (5)$$

NB: This numerical analysis presents an initial work on the accuracy of air temperature measurements. CFD simulations and experimental data are needed to further validate the calculation and the assumptions.

Without solar radiation:

When measuring air temperature without solar radiation, the radiation in the room is lower and such a complex set-up (shield and fan) might not be needed. The purpose of this part is thus to evaluate different set-up to measure air temperature without solar radiation. Three different set-up will be tested numerically:

- Bare thermocouple without silver-coating (ε = 0.20)
- Bare thermocouple with silver-coating (ε = 0.06)
- Thermocouple with silver-coating (ε = 0.06) and silver-shield (ε = 0.06)

For the first two cases, the heat balance of the thermocouple differs from the previous part (Figure 16). The radiative exchange is calculated assuming concentric spheres.

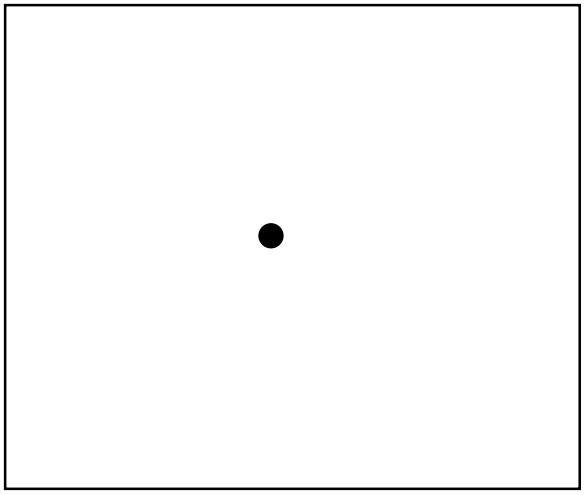

Room:
$\varepsilon = 0.9$

Thermocouple:
h_{conv} = 18 W/m^2.K @ 0.2 m/s
14 W/m^2.K @ 0.1 m/s
10 W/m^2.K @ 0.05 m/s [23]
$\varepsilon = 0.06$ or 0.20

Figure 16: Top view of the thermocouple and the room (not at the right scale). The boundary conditions for the calculation are given in the table on the right.

The results from the heat balance are shown in Figure 17. It can be observed that a silver-coated thermocouple ($\varepsilon = 0.06$) has a lower sensitivity to radiation than a classic thermocouple. But the shielding technique seems to be the most efficient technique to get accurate measurement of the air temperature.

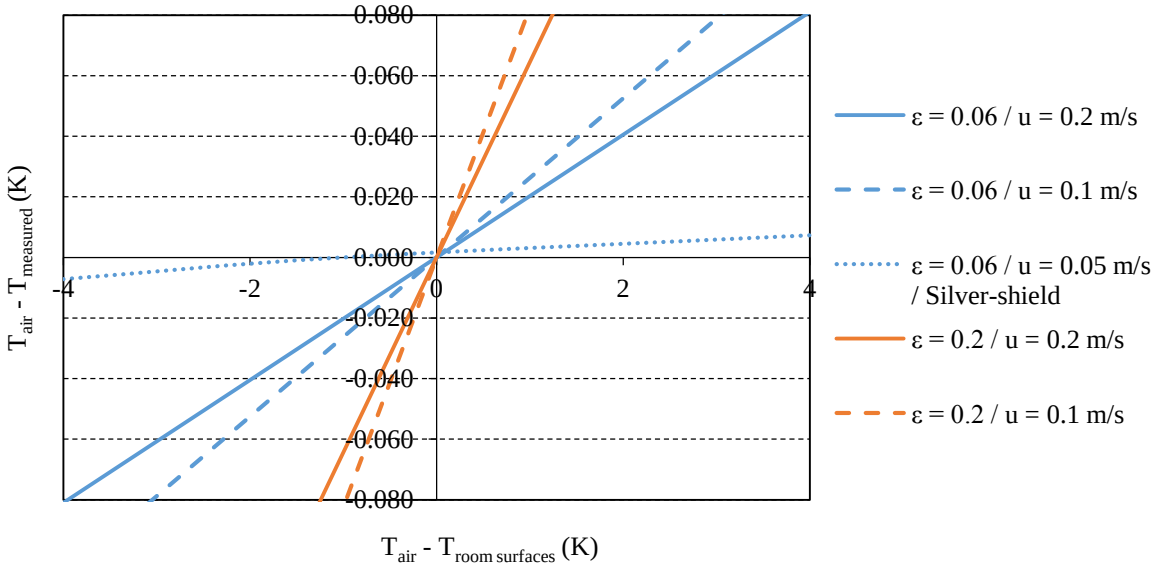

Figure 17: Difference between measured and air temperature for various temperature differences between the air and the room surfaces and various set-up.

Similar analysis has been performed by Goethals et al. [15] with bare thermocouples without silver-coating. They found differences between 0.05 up to 0.1 K for experiments with night-time ventilation, but no information was given on the temperature difference between the air and the surrounding surfaces.

NB: This numerical analysis presents an initial work on the accuracy of air temperature measurements. CFD simulations and experimental data are needed to further validate the calculation and the assumptions.

4) Cooling effect from the radiant wall

A one-dimensional finite volume model with an explicit scheme [16] has been used to determine the conductive heat flux at each section of the test room. The surface temperature and the temperature difference inside the construction over a 30-mm layer of EPS have been used as boundary conditions of the calculation. But a temperature difference cannot be used directly as boundary condition in the numerical model. A heat flux is required. Therefore, a linear temperature profile through the thermopile is first assumed (steady-state conditions) and then the heat flux is modified until the measured temperature difference matches the calculated one.

For modelling conduction when the radiant panels are activated, the same numerical model has been used, adding an internal heat source inside the construction layers. As the numerical model is one-dimensional, an equivalent-layer has been defined to model correctly the two-dimensional heat flow around the pipes (Figure 18). In order to define the properties of this equivalent layer (λ, ρ, C_p), the exact two-dimensional geometry has been modelled with a commercial program using FEM technique [17]. Steady state calculations have been performed to define the equivalent thermal conductivity and dynamic calculations (sinusoidal variations of the boundary conditions) have been done to determine the equivalent thermal capacity. The results are presented in Table 3.

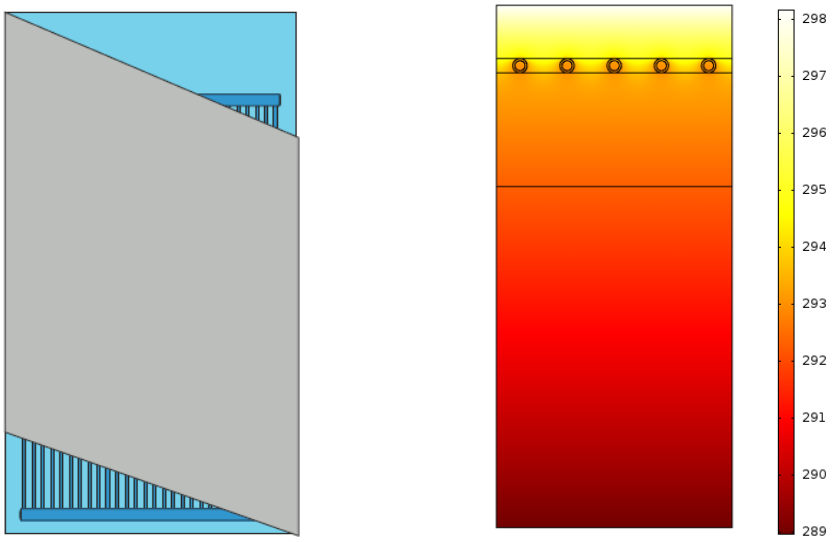

Figure 18: Front view of the radiant panel (on the left) and cross section of the construction (on the right).

Table 3: Thermal properties of the equivalent layer (thickness 3.35 mm).

Type of model	Material	λ (W/m.K)	ρ (kg/m³)	C_p (J/kg.K)
2D	Extruded polystyrene	0.035	40	1450
	Propylene	0.24	905	1800
	Water (14°C)	0.584	999.5	4193
1D equivalent	-	0.060	256	1833

To evaluate the accuracy of such a simplification, the model has been tested using the experimental boundary conditions of one typical day. The calculation has been performed in parallel with the exact two-dimensional geometry and with the equivalent layer model. The repartition of error is given in Figure 19: the accuracy of the model can be estimated to ± 7.7 %. When deriving the equivalent properties, a better accuracy had been observed due to "smoother" boundary conditions.

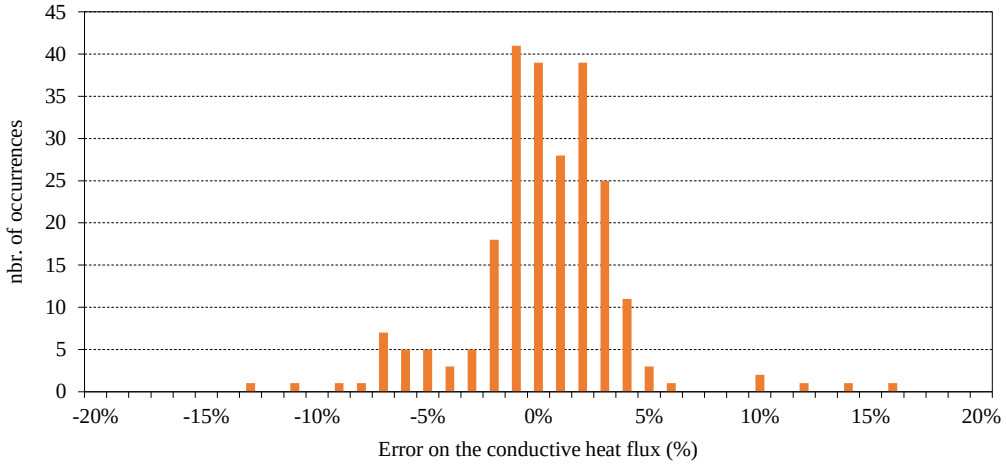

Figure 19: Error distribution on the calculation of the conductive heat flux inside the experimental room with the 1D-equivalent layer model (5th of July, surface nbr. 18).

5) Summary of the measurement uncertainties

Table 4: Data loggers properties

	Module	Nbr channels	Range of measurement	Resolution	Accuracy	Logging frequency
Fluke Helios 2680	PAI	120	± 90 mV	*0.0003 mV*	$\pm \frac{2}{3} \cdot (7 + 0.01\%)\ \mu V$	0.3 Hz
Fluke Helios 2287A	161	100	± 64 mV	*0.0006 mV*		0.1 Hz
HBM CP32B	AP801	25	± 10 V	0.001 V	± 0.05 %	10 Hz

Table 5: Temperatures measured during the experiments.

	Location	Type of sensor	Nbr. of sensors	Accuracy
Thermopiles	Inside the construction	Type K with 4 junctions	80	± 0.07 K
Surface temperature	Opaque surfaces	Type K, Painted	80	± 0.15 K
	Transparent surfaces	Type K, Covered with a reflective tape	4	± 0.15 K without sun or ± 0.30 K [18]
Air temperature	Experimental room	Type K, Silver-coated, With a silver shield mechanically ventilated	25	± 0.15 K + Equation 5
	Guarded zone, Outdoor		2	± 0.15 K
	Inlet, Outlet	Type K, Silver-coated, With a silver shield	2	± 0.15 K
Operative temperature	0.1, 0.6 and 1.1 m	Type K, With a 40-mm-diameter grey globe	3	± 0.30 K [19]

Table 6: Weather data measured during the experiments.

	Location	Type of sensor	Accuracy
Ratio of diffuse to total solar radiation	Horizontal surface	DeltaT BF3 (400 to 700 nm)	± 19 %
Solar global irradiance	Facade	Kipp & Zonen CMP 21 (285 to 2800 nm)	± 3 %
Solar global irradiance	After the glazing	Kipp & Zonen CMP 22 (200 to 3600 nm)	± 2 %
Wind speed	Beside the facade (10 m high)	3D ultrasonic anemometer WindMaster	± 1.5 %

Table 7: Other parameters measured during the experiments.

	Type	Type of sensor	Accuracy
Heat flow from the panels and chilled beam	Water temperature	Pt 500	± 0.057 K
	Water flow	Brunata HGQ1 – R0	± 0.9 L/h
Comfortina	Surface temperature (skin)	Nickel wires	± 0.2 K [20]
	Surface temperature (clothes)		± 0.5 K
	Heat flux		± 1 % [20]
Air velocity	Mean air velocity	Dantec 54R10 Hot sphere	± max (0.05 , 0.01+5%)
	Turbulence intensity	Dantec 54R10 Hot sphere	± (4 + 23%) [21]
Air flow	Inlet	EHBA Ø 125 mm	± 7.5 %
Humidity	Inlet/Outlet	Honeywell HIH-4000-03	± 7.5 %

II. Sensitivity analysis

In order to evaluate the sensitivity of the heat balance to the experimental parameters, a differential sensitivity analysis has been performed. In turn, each of the 87 experimental parameters has been changed to its "$\mu+2\sigma$" value and the effect on the heat balance has been observed. This type of investigation is a rather simple and straightforward method. But the possible correlation and/or unlinearity will not be taken into account.
The different experimental measurements and their associated uncertainties have been described in the previous sections. In addition to these parameters, uncertainty on the geometrical properties has been taken into consideration: room dimension (± 0.02 m), thickness of the layers (± 0.001 m). A model for infiltration between the room and the guarded zone and the room and outdoor has also been implemented, based on the measurements of pressure difference and the results of the blower door tests.

Two sensitivity analysis have been performed, one when the radiant wall is active and one with the active chilled beam. The results are presented in Table 8. It can be observed that there are similarities for the two cooling systems: the optical properties of the glazing, the measurement of the cooling power from the activated element, the measurement of solar radiation and the evaluation of the ventilative flow influence the most the accuracy of the heat balance. The uncertainties on the modelisation of the 2D heat flow through the activated pipes also influences the accuracy of the heat balance of radiant panels.

Table 8: Summary of the ten parameters, which influence the most the heat balance (expressed in percentage of the gains or losses).

Radiant panel		Active chilled beam	
Equivalent layer pipes	5.0	Window - Tsol	4.3
Window - Tsol	4.7	Window - Abs2	2.8
Act elemt - flow	3.6	Act elemt - tmp return	2.8
Window - Abs2	3.1	Act elemt - Tmp in	2.6
Act elemt - tmp return	2.7	Ventil - flow	1.5
Act elemt - Tmp in	2.6	Rho/Cp - Gyp	1.3
Ventil - flow	1.4	Rho/Cp - Equip (V)	1.3
Rho/Cp - Gyp	1.4	Air tmp - Inlet	1.1
Air tmp - Inlet	1.2	Air tmp - Outlet	1.1
Air tmp - Outlet	1.2	Pyranometer outside	1.1

III. Experimental calculation of the uncertainty on the heat balance

The room heat balance has been performed for a time-step of 30 seconds and is expressed by Equation 6. The conduction and short-wave radiation are evaluated for each of the 83 sub-surfaces. The left part of the equation corresponds to the change of internal energy in the room, which includes both the capacitance of the air and of the equipment. The temperature swing of the equipment is assumed to follow the variation of the air temperature. The thermal mass of the equipment has been calibrated using the experimental results and is equal to 4.7 Wh/m^2_{floor}.K.

$$\left(V_{room}\,\rho_{air}\,C_{p\,air} + C_{m\,equipment}\right)\frac{\partial T_{air}}{\partial t} = \sum_{i} Q_{cond\,i} + Q_{rad\,SW} + Q_{thermal\,manikin} + Q_{equipment} + Q_{ventilation} + Q_{chilled\,beam} \qquad (6)$$

By comparing the sum of the gains to the sum of the losses, it is possible to check the accuracy of both the measurements and the method of analysis. An example of heat balance is given in Figure 20.

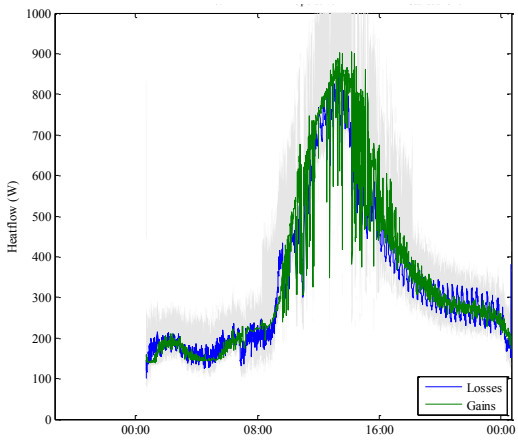

Figure 20: Heat balance of the test room over 24 hours with the radiant wall activated.

The comparison of gains and losses has been performed for different intervals of calculation (Figure 21). The uncertainty on a single measurement point (i.e. representing 30 seconds of experiment) follows a normal distribution and $\Delta q_{\%} = \pm 29$ % (result based on around 161 000 data points). This uncertainty did not show any correlation with the type of terminal or with the intensity of solar radiation. For 30-minute averaged data, the accuracy $\Delta q_{\%}$ is decreasing down to ± 18 %.

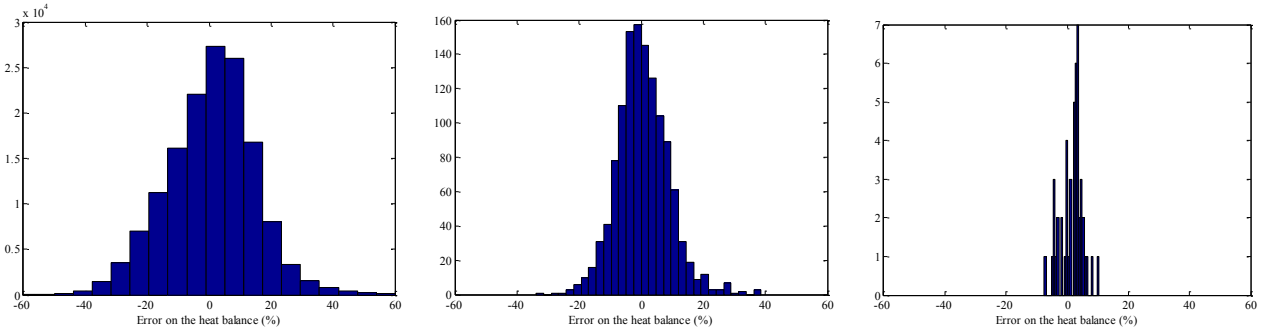

Figure 21: Histogram of the error on the heat balance for 30-seconds average (on the left), for hourly-average (in the center) and daily average (on the right).

Table 9: Summary of the uncertainty on the heat balance

Interval of analysis	Uncertainty experimentally observed
30 seconds	± 29 %
30 minutes	± 18 %
1 hour	± 17 %
1 day	± 7 %

IV. List of experimental data

1) Experiments – Steady-state

Exp. Nbr.	Cooling elmt.	Operative tmp (°C)	Air tmp (°C)				Surf tmp (°C)				Ext tmp (°C)	Guarded tmp (°C)	Heat loads (W)		Ventilation (ACH)	Cooling system		
			Room	Inlet Room	Inlet Lab	Outlet	Room average	Comf.	Carpet	Panel			Carpet	Comf.		Flow (m^3/h)	T_{in} (°C)	T_{out} (°C)
35	ACB	24.87	23.9	17.3	20.8	23.3	25.6	29.3	35.7	NaN	4.2	19.6	374.0	52.5	2.20	0.107	13.5	15.9
36	ACB	26.00	25.0	18.4	27.5	24.5	26.7	29.9	36.7	NaN	9.4	26.5	358.2	45.8	2.28	0.168	11.4	13.6
37	Radiant	26.00	26.4	27.2	27.3	27.1	26.5	30.1	37.1	20.2	10.6	26.3	350.1	42.5	2.14	0.025	12.1	14.4
38	Radiant	25.95	26.2	26.3	25.6	26.7	26.4	30.1	37.2	20.5	4.1	24.5	361.3	42.5	2.23	0.022	12.7	15.1
39	ACB	26.03	25.1	18.3	25.6	24.5	26.8	30.0	36.6	NaN	5.8	24.5	356.7	45.1	2.16	0.112	11.9	14.8
40	ACB	26.08	25.1	18.2	23.7	24.5	26.8	30.0	36.7	NaN	12.0	22.6	361.0	45.2	2.15	0.111	13.0	15.7
41	Radiant	25.95	26.0	25.3	23.6	26.2	26.3	30.1	37.0	21.0	7.7	22.5	365.9	43.1	2.23	0.025	14.6	16.4
42	Radiant	25.91	25.8	24.5	21.9	25.8	26.3	30.0	37.2	21.3	6.1	20.7	373.6	43.5	2.24	0.022	15.3	17.2
43	ACB	26.06	25.1	19.0	21.8	24.6	26.7	30.0	36.8	NaN	6.9	20.6	373.0	45.0	2.23	0.107	15.7	18.0
44	Radiant	25.99	26.0	25.4	23.7	26.2	26.3	30.1	37.2	20.9	7.2	22.6	368.9	42.9	2.26	0.028	14.4	16.0
45	Radiant	25.99	26.1	25.8	24.6	26.4	26.4	30.1	37.4	20.7	11.6	23.5	369.2	42.5	2.31	0.026	13.7	15.5
46	Radiant	26.04	26.2	26.3	25.6	26.7	26.4	30.1	37.2	20.5	6.4	24.5	357.8	42.6	2.22	0.025	13.0	15.1
47	Radiant	25.94	26.2	26.7	26.3	26.7	26.4	30.1	37.1	20.2	9.7	25.3	354.5	43.0	2.24	0.025	12.4	14.6
48	ACB	26.07	25.2	18.6	24.7	24.6	26.8	30.0	36.5	NaN	3.5	23.6	355.9	45.3	2.15	0.111	13.1	15.8
49	ACB	26.11	25.2	19.0	23.8	24.7	26.8	30.0	36.8	NaN	4.4	22.7	368.2	45.2	2.30	0.110	14.3	16.9
50	ACB	26.03	25.1	18.4	26.6	24.5	26.7	30.0	36.4	NaN	3.5	25.5	353.3	45.6	2.22	0.121	11.5	14.4
80	ACB	26.11	24.9	21.8	24.9	24.8	26.3	29.7	35.0	NaN	15.0	23.7	361.2	50.5	3.21	0.135	15.2	17.7
81	ACB	26.08	24.9	22.1	25.9	24.8	26.3	29.7	34.7	NaN	17.0	24.7	358.4	47.6	3.59	0.105	15.3	18.7
82	ACB	26.95	25.8	20.2	25.9	25.5	27.3	30.3	36.0	NaN	13.4	24.7	355.8	42.0	1.98	0.167	13.0	14.9
83	ACB	29.64	28.6	21.2	25.9	29.0	30.0	31.9	38.2	NaN	9.0	24.7	353.0	24.0	1.16	0.166	13.0	14.4
84	Radiant	26.28	26.1	26.2	25.8	26.3	26.2	29.9	35.4	20.7	8.4	24.6	353.7	41.8	3.60	0.040	13.0	14.4

2) Experiments – Dynamic

The conditions are changing over the days, both in the test-room and outside. It is thus difficult to give more detailed values than the one presented below:

Exp. Nbr.	Cooling elmt.	Nbr. of days + Type of weather	Operative tmp (°C) Max	Min	Ventilation (ACH)	Guarded zone tmp (°C)	Outdoor tmp at night (°C)
121	ACB	4 (1 gray - 2 gray - 3 gray – 4 sunny)	27	23	2.4	25	12
122	Radiant	4 (1 gray - 2 cloudy - 3 rain a bit & sunny – 4 gray)	27	21.5	2.4	25	11
123	Radiant	2 (1 gray rain - 2 rain)	25	21	2.4	25	9
124	Radiant	5 (sunny all days)	30	22	2.4	25	11
125	ACB	11 (sunny, except days 4 and 5)	30	22	2.4	25	14
126	Radiant	6 (1,2,3 sunny – 4,5,6 gray)	31	22	2.4	25	16
127	ACB	7 (1,2,4 cloudy – 3,5,6,7 gray)	28	22	2.4	25	15
129	ACB	3 (1 gray – 2 rainy – 3 sunny)	30	22	2.4	25	10
130	Radiant	9 (1,2,3,4 cloudy – 5,6,7,8,9 sunny)	32	22	2.4	25	11
131	AC	1 (gray)	25	22	2.4	25	11

3) Structure of the data

The experimental data are gathered in two main folders, which are described below. The analysis has been performed using the commercial software Matlab.

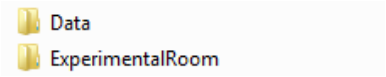

The experimental room properties are given in the folder "ExperimentalRoom":

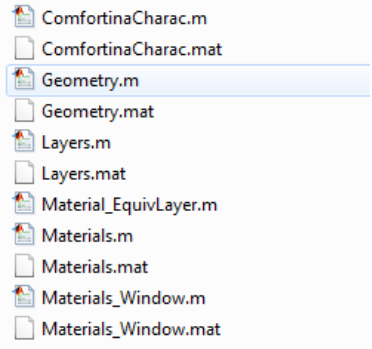

For each experiment, the following data are available (in "Data\Exp_XXX").

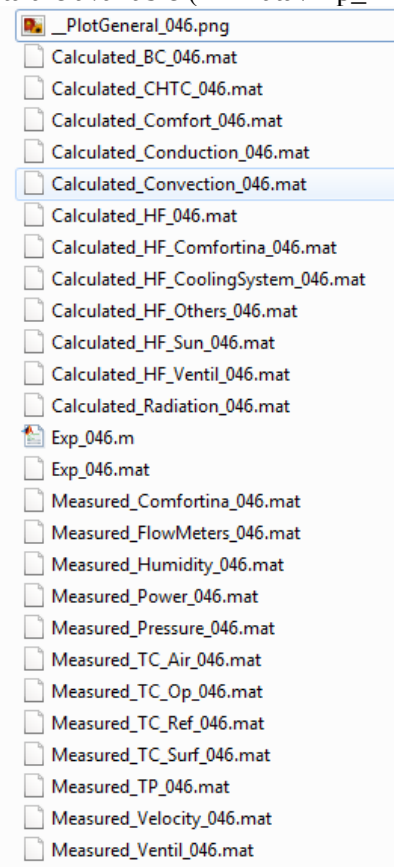

There are four types of data in this folder:

- "Exp_XXX" gives general information about the experimental parameters
- "Measured_" corresponds to the measured data (after applying the calibrations and removing the outliers)
    - TC corresponds to thermocouple
    - TP corresponds to thermopile

- "Calculated_" corresponds to data after post-processing (averaged over 30 seconds and heat flow calculated)
    - BC corresponds to boundary conditions
    - CHTC corresponds to convective heat transfer coefficient
    - HF corresponds to heat flow
- Finally, a set of graph is given to get an overview of the different experimental parameters (in "Data\Exp_XXX__PlotGeneral_XXX.png"):

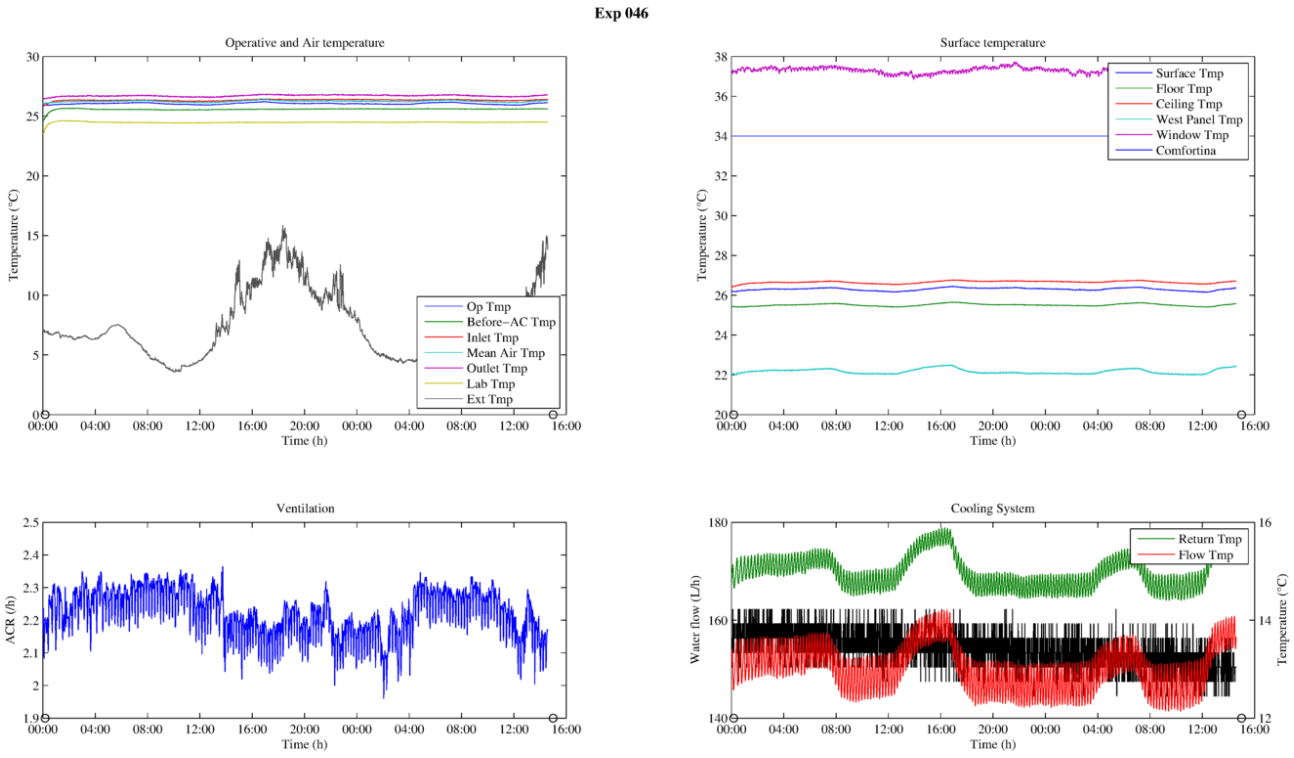

4) Data

The data can be accessed from VBN (http://vbn.aau.dk/en/persons/pp_a63f4ea1-492d-49f6-a6f7-0eec3c7e1893/publications.html). If you are using these measurements in your publication, please make a reference to:

- J. Le Dréau, P. Heiselberg, R.L. Jensen, A full-scale experimental set-up for assessing the energy performance of radiant wall and active chilled beam for cooling buildings, Building Simulation: An International Journal (2014).
- J. Le Dréau, P. Heiselberg, R.L. Jensen, Experimental investigation of the influence of the air jet trajectory on convective heat transfer in buildings equipped with air-based and radiant cooling systems, Journal of Building Performance Simulation (2014).

For further information about the experiments, please contact:

- Jérôme Le Dréau (jld@civil.aau.dk)
- Per Heiselberg (ph@civil.aau.dk)
- Rasmus Lund Jensen (rlj@civil.aau.dk)

References

[1] J. Le Dréau, P. Heiselberg, R.L. Jensen, A full-scale experimental set-up for assessing the energy performance of radiant wall and active chilled beam for cooling buildings, Building Simulation: An International Journal (2014).

[2] J. Le Dréau, P. Heiselberg, R.L. Jensen, Experimental investigation of the influence of the air jet trajectory on convective heat transfer in buildings equipped with air-based and radiant cooling systems, Journal of Building Performance Simulation (2014).

[3] Wikipedia, Accuracy and precision. 2013 (2013).

[4] A. Janssens, S. Roels, L. Vandaele, Full scale test facilities for evaluation of energy and hygrothermal performances (2011).

[5] M.B. Nielsen, Kaliebreringscertifikat (in Danish). Teknologisk Institut (16 November 2012).

[6] Isothermal Technology, Venus 2140: Evaluation Report – Issue 02 (2000).

[7] KAYE Instruments, Thermocouple Reference Systems. Bedford, Massachusetts, US.

[8] M. Carroll, W.F. Guthrie, G.W. Burns, M. Kaeser, G.F. Strouse, NIST ITS-90 Thermocouple Database., National Institute of Standards and Technology (NIST), U.S. Commerce Department (2013).

[9] Fluke, 2680 Series. Data Acquisition Systems – Technical data. (2002).

[10] N. Artmann, R. Vonbank, R.L. Jensen, Temperature measurements using type K thermocouples and the Fluke Helios Plus 2287A data logger, DCE Technical Reports No. 52. Aalborg University (2008).

[11] MathWorks, Matlab - Interpolation (griddata.m) (2011).

[12] O. Kalyanova, F. Zanghirella, P. Heiselberg, M. Perino, R.L. Jensen, Measuring air temperature in glazed ventilated façades in the presence of direct solar radiation. The International Conference on Air Distribution in Rooms, Roomvent (2007).

[13] O. Kalyanova, P. Heiselberg, Experimental Set-up and Full-scale measurements in the Cube, DCE Technical Reports No. 34. Department of Civil Engineering, Aalborg University (2008).

[14] R. Kurzeja, Accurate temperature measurements in a naturally-aspirated radiation shield, Bound. -Layer Meteorol. 134 (2010) 181-193.

[15] K. Goethals, M. Delghust, G. Flamant, M. De Paepe, A. Janssens, Experimental investigation of the impact of room/system design on mixed convection heat transfer, Energy Build. 49 (2012) 542-551.

[16] S.V. Patankar, Numerical heat transfer and fluid flow, Taylor & Francis (1980).

[17] C. Multiphysics, Version 4.3, COMSOL, Inc., USA (2012).

[18] H. Manz, P. Loutzenhiser, T. Frank, P.A. Strachan, R. Bundi, G. Maxwell, Series of experiments for empirical validation of solar gain modeling in building energy simulation codes—Experimental setup, test cell characterization, specifications and uncertainty analysis, Build. Environ. 41 (2006) 1784-1797.

[19] R. Tomasi, M. Krajčík, A. Simone, B.W. Olesen, Experimental evaluation of air distribution in mechanically ventilated residential rooms: Thermal comfort and ventilation effectiveness, Energy Build. 60 (2013) 28-37.

[20] PT Teknik, Comfortina, http://pt-teknik.dk/ (1999).

[21] A.K. Melikov, Z. Popiolek, M.C.G. Silva, I. Care, T. Sefker, Accuracy Limitations for Low-Velocity Measurements and Draft Assessment in Rooms, HVAC&R Research. 13 (2007) 971-986.

[22] EN 15265:2007, Energy performance of buildings - Calculation of energy needs for space heating and cooling using dynamic methods. General criteria and validation procedures (2007).

[23] V.T. Morgan, The overall convective heat transfer from smooth circular cylinders, Advances in heat transfer. 11 (1975) 199-264.

[24] ASHRAE, ASHRAE – Handbook Fundamentals – Chapter 4: Heat Transfer, American Society of Heating, Refrigeration and Air-Conditioning Engineers Inc., Atlanta, GA. (2009).

ISSN 1901-726X
DCE Technical Report No. 168